# A state estimate of the routes of the upper branch of the Atlantic Meridional Overturning Circulation

**Louise Rousselet**[1], **Paola Cessi**[1]*, **Gael Forget**[2]

[1]Scripps Institution of Oceanography, University of California, San Diego, USA
[2]Dept. of Earth, Atmospheric and Planetary Sciences, Massachusetts Institute of Technology, Cambridge, MA, USA

**Key Points:**

- The upper limb of the meridional overturning circulation originates primarily from the Tasman Leakage and the Indonesian Throughflow
- 97% of the upper limb of the meridional overturning circulation enters the Atlantic from the Agulhas region, around the tip of South Africa
- Because its upper limb is saltier than its lower limb, the overturning exports freshwater out of the Atlantic basin.

*Paola Cessi, Scripps Institution of Oceanography,
University of California, San Diego,
La Jolla, CA 92039-0213, USA

Corresponding author: Paola Cessi, pcessi@ucsd.edu

**Abstract**

The origins of the upper branch of the Atlantic Meridional Overturning Circulation (AMOC) are traced with backward-in-time Lagrangian trajectories, quantifying the partition of volume transport between different routes of entry from the Indo-Pacific sector into the Atlantic. Particles are advected by a three-dimensional, incompressible velocity field from a recent release of "Estimating the Circulation and Climate of the Ocean" (ECCOv4). This global time-variable velocity field is a dynamically consistent interpolation of over one billion oceanographic observations collected between 1992 and 2015. Of the 13.6 Sverdrups (1Sv = $10^6$ $m^3/s$) of upper and intermediate water flowing northward across 6°S, 15% enters the Atlantic from Drake Passage, 35% enters from the straits between Asia and Australia, termed the Indonesian Throughflow, and 49% comes from the region south of Australia, termed the Tasman Leakage. The salinity budget shows that the AMOC exports freshwater out of the Atlantic.

## Plain Language Summary

Particle trajectories in the upper limb of the Atlantic Meridional Overturning Circulation (AMOC) are traced from the equatorial Atlantic to different sections of origin in the Southern Ocean. The three-dimensional velocity moving the particles is an estimate combining over a billion of observations with a global ocean model that conserves mass, momentum, temperature, salinity and sea-ice over a regular grid. 97% of the particles enter the Atlantic from the tip of South Africa, as a relatively warm and salty water mass, while the remaining 3% enters from the tip of South America cold and fresh. Because the upper limb of the AMOC entering the Atlantic is saltier than the exiting lower limb, this estimate shows that the AMOC might collapse given appropriate freshwater perturbations.

## 1 Introduction

The meridional overturning circulation (MOC) of the Ocean is a key component of Earth's climate system. The Atlantic-sector MOC transports heat northwards at all latitudes (Hsiung, 1985), modulating the position of the Inter Tropical Convergence Zone (Kang et al., 2008).

The MOC includes northward flow of intermediate and upper waters from the Southern Ocean into the Atlantic, which are eventually transformed into North Atlantic Deep Water (NADW) in the Labrador and Nordic Seas. NADW then flows southward at depth upwelling in the Southern Ocean to close the *mid-depth cell* (red contours in figure 1). An equivalent mid-depth cell is absent in the Indo-Pacific sector (Cessi, 2019).

Water that has upwelled from the lower, southward branch of the mid-depth cell in the Indo-Pacific sector (south of 30°S) can return to the North Atlantic through two pathways: the *warm route*, i.e. *westward and northward around the tip of South Africa* (Gordon, 1986), or the *cold route*, i.e. *eastward and northward around Drake Passage* (Rintoul, 1991). The quantitative contributions of these two routes differ among estimates, but this partition is important for the transport of heat and freshwater into the Atlantic. Water that enters the South Atlantic through the warm route is warm and salty, while that entering through the cold route is fresh and cold. Many model simulations have shown that if the cold route prevails, the MOC is robust to freshwater perturbation in the high latitudes of the North Atlantic and Arctic. Vice versa, if the exchange is mostly via the warm route, then North Atlantic freshwater perturbations shut down the MOC (de Vries & Weber, 2005; Beal et al., 2011; Drijfhout et al., 2011).

Several observational and numerical studies have estimated the relative contribution of the two routes. Most observational studies support the cold water route (Schmitz Jr, 1995; Macdonald, 1998; Sloyan & Rintoul, 2001; Talley, 2013), while most numerical studies and one observational analysis favor the warm water route (Speich et al., 2001; Holfort & Siedler, 2001; Donners & Drijfhout, 2004; Speich et al., 2007; Rodrigues et al., 2010; Cessi & Jones, 2017; Rühs et al., 2019). Donners and Drijfhout (2004) illustrate the difficulty of establishing the origin of the MOC's upper branch using inverse models with sparse observations at hydrographic sections: this method applied to the output of an eddy-resolving computation leads to a qualitatively different partition between routes than that obtained with Lagrangian analysis.

A major difficulty with identifying routes of the upper branch of the MOC is that inter-basin connection is mediated by currents in the Southern Ocean, which are dominated by a recirculating component associated with the Antarctic Circumpolar Current (ACC) (Forget & Ferreira, 2019). The ACC recirculates about 50 Sv (1 Sv = $10^6$ $m^3$/s) in the top 1000 meters of the water column, while the upper branch of the MOC carries about 14Sv, a small fraction of the recirculating transport (Cessi, 2019).

To overcome this difficulty, we quantify the pathways of intermediate water from the Indo-Pacific to the Atlantic using Lagrangian analysis. The method consists of tracking particle trajectories backwards in time from an "exit" section in the South Atlantic (here 6°S) to specific "entry" sections. The origin of particle trajectories is identified by the backward-in-time first passage through one of the "entry" sections. The quantification of mass transport with particle trajectories is performed by initially populating the exit section with a large number of particles whose concentration is proportional to the local transport. Each particle carries a small amount of transport that is conserved following the trajectory because the velocity vector field conserves mass (volume). This type of calculations has been successfully performed using velocity fields from ocean general circulation models (Döös, 1995; Speich et al., 2001; Rühs et al., 2019), but not with global observations. To estimate Lagrangian transport, it is necessary to have velocities interpolated over a global grid, tightly constrained by observations, while strictly conserving mass. A product that satisfies these requirements is the three-dimensional, time-variable, incompressible velocity from "Estimating the Circulation and Climate of the Ocean" (ECCOv4) (Forget, Campin, et al., 2015; Fukumori et al., 2017).

The modern measure of the MOC is given in terms of the "residual" transport within isopycnal layers, rather than depth layers. The residual overturning circulation measures the (potential) density transport, rather than the volume transport: it is more meaningfully associated with the transport of tracers than is the overturning in depth coordinates (Young, 2012). Specifically, the residual overturning circulation captures the transport effected not only by the average meridional velocity but also by waves, eddies, and gyres with zero time- or zonally averaged velocity.

In models that do not fully resolve mesoscale processes, the eddy-flux of tracers needs to be parametrized. The parametrized eddy-transport is typically expressed in terms of isopycnal diffusion and a "bolus" velocity related to the slope of isopycnals (Redi, 1982; Gent & McWilliams, 1990; Griffies, 1998). In these models the appropriate way to calculate the residual transport of the MOC is to use the sum of Eulerian velocity plus the bolus velocity, integrated over density layers rather than depth layers. In figure 1, the time-averaged and longitudinally integrated MOC is calculated in density coordinates and latitude, using $\sigma_2$, i.e. potential density referred to 2000 decibars, as the vertical coordinate. Accordingly, the velocity used to calculate Lagrangian trajectories is the sum of Eulerian velocity plus the bolus velocity in all three dimensions.

## 2 Calculation of Lagrangian trajectories

The velocities used in the calculation of Lagrangian trajectories are the monthly climatology available in the release 3 of ECCOv4 on the native model grid at 1° horizontal resolution (the *Lat-Lon-Cap*-90 grid as defined in Forget, Campin, et al. (2015)) and with 50 vertical levels (Forget, Campin, et al., 2015; Fukumori et al., 2017). These velocities derive from the dynamically-consistent assimilation of over one billion observations for the period 1992-2015 into a primitive-equations ocean-sea-ice model that satisfies exact conservation laws for mass, temperature, salinity and sea-ice.

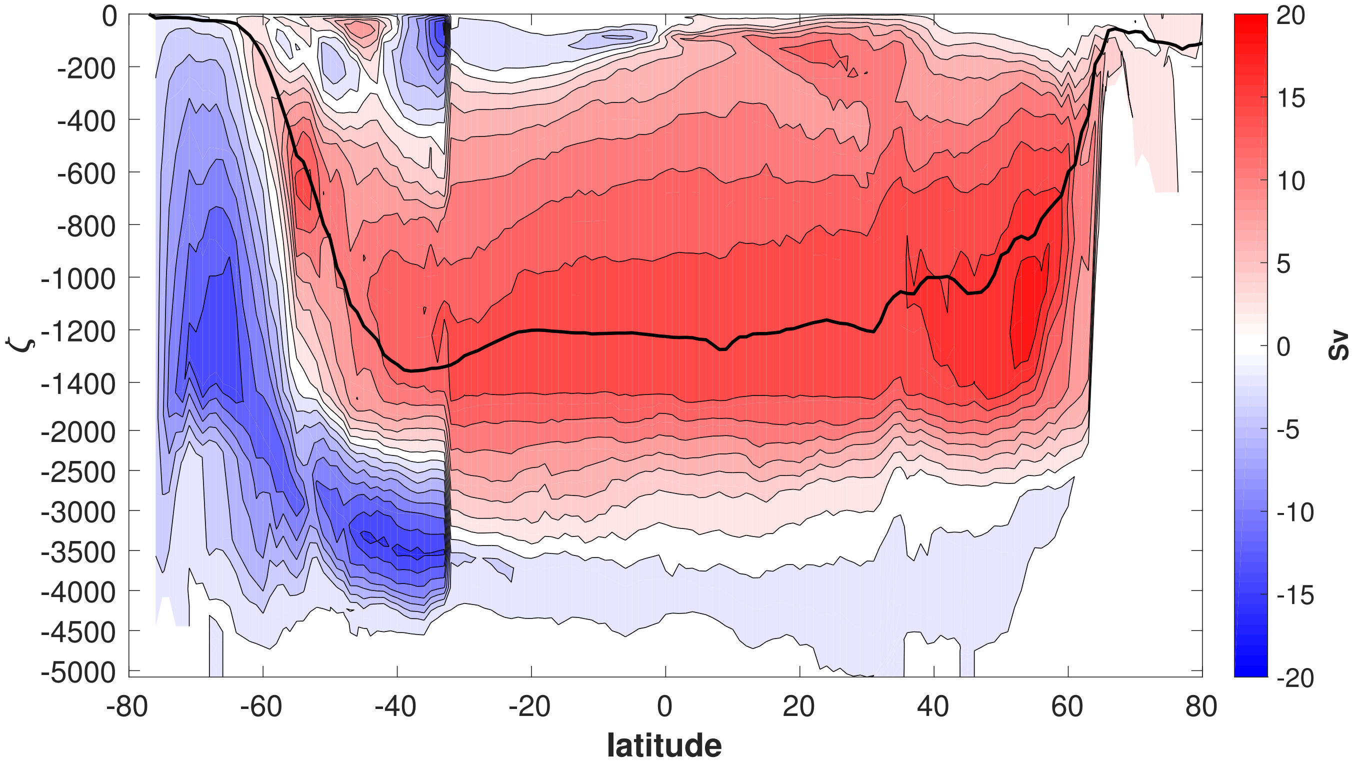


**Figure 1.** Residual meridional overturning circulation vertically integrated above surfaces of constant $\sigma_2$, then time averaged and zonally integrated in the Southern Ocean south of 37°S, and in the Atlantic sector north of 37°S, as a function of latitude (abscissa) and $\sigma_2$ (ordinate). The ordinate is remapped into a depth-like coordinate $\zeta$(latitude,$\sigma_2$) which represents the time and zonal averaged (over all longitudes) depth of each $\sigma_2$ surface. The ECCO4 (release 3) horizontal velocity (Eulerian+bolus), temperature and salinity re-analysis fields are used. Positive values (red) indicate clockwise circulation. The contour interval is 2 Sv (1 Sv = $10^6$ m$^3$/s). The thick black line marks the depth $\zeta$(latitude,$\sigma_2$=36.6 kg/m$^3$), which approximately divides the upper and lower branches of the residual MOC.

The assimilated data consist of satellite products (including along-track altimetry, mean dynamic topography, remotely sensed ocean bottom pressure, sea-surface temperature, sea-ice concentration and surface salinity), and temperature and salinity profiles collected in-situ (including from all Argo floats). To minimize misfit between the model and the observations, the following model parameters are optimized (Forget, Campin, et al., 2015; Fukumori et al., 2017): initial conditions in January 1992, air-sea interactions throughout 1992-2015, diapycnal and isopycnal tracer diffusion rates, and the parameterized advective effect of mesoscale eddies (Gent & McWilliams, 1990; Forget, Ferreira, & Liang, 2015). Because the optimization uses the adjoint and forward versions of the model, for fifty iterations, the adjustment of the control parameters can be effected and beneficial on a time-scale of hundreds of years, even though the data record is only 24 years long (Forget, Ferreira, & Liang, 2015).

Many studies have looked at various measures and methods to assess the ECCOv4 estimate, which collectively affirm its value for understanding both the Ocean climatology and its variability from observations (Forget, Campin, et al., 2015; Fukumori et al., 2017; Forget & Ponte, 2015; Forget & Ferreira, 2019; Jackson et al., 2019). The estimate of the MOC according to ECCOv4 is in broad agreement with several independent (i.e. not assimilated) estimates [see Table 1 in Cessi (2019)]. The ACC transport at Drake Passage in ECCOv4 is 155 Sv which is intermediate between the two recent independent ‘in-situ‘ estimates of Cunningham et al. (2003) (134 ± 11 Sv) and Donohue et al. (2016) (173 ± 11 Sv), and in the middle of the estimates compiled by Uotila et al. (2019).

To determine the Lagrangian trajectories, the ECCOv4 climatological monthly velocities are interpolated in space using an incompressibility-preserving, transport-weighted algorithm (Döös, 1995; Blanke & Raynaud, 1997) and advected backward in time using a Runge-Kutta fourth-order scheme for 2011 years (more details in the supplemental material). Because the climatological monthly velocities are one-year periodic, the annual cycle can be repeated as many times as needed. Particles are initialized every month for one year (for a total of 63482 particles) at 6°S in the South Atlantic, at depths above the $\sigma_2 = 36.6\text{kg/m}^3$ surface: this defines the "exit section". The $\sigma_2 = 36.6\text{kg/m}^3$ surface marks the lower boundary of the upper, northward branch of the MOC. Each particle carries about $2 \times 10^{-4}$ Sv so that the number of particles per each grid-face on the section is proportional to the transport of that grid-face (the exact transport of each particle is recorded). Because the three-dimensional velocity vector is exactly incompressible, the transport of each particle is conserved following the trajectory (Döös, 1995; Blanke & Raynaud, 1997). This conservation can be used to quantify the transport through different "entry" sections, determining the origin of waters that feed the upper branch of the MOC. The place and time of origin is defined as being the first passage from the exit to one of the four entry sections going backward in time.

The entry sections at which we measure the first-passage are at Drake Passage (DP, at 66°W), at the Indonesian Throughflow (IT, at 116°E), at the Tasman leakage region (TL, at 116°E) and in the South Atlantic at 6°S for depths below the $\sigma_2 = 36.6$ kg/m$^3$ surface, i.e. in the lower limb of the MOC (cf. figure 2). The northward transport at the "exit" section is 13.64 Sv. The particles are followed backward in time for 2011 years, after which all but 0.3% have moved through one of the entry sections. The region encompassed by the entry and exit sections has a net evaporation of 0.44Sv, but our procedure does not allow particles to exit or enter the air-sea boundary: instead particles that try to escape the surface are reinjected into the first model level. The computation was repeated for 512 years with double the number of particles (126964), and the transport values at the exit region differ at most by 0.2% over that time from those with 63482 particles. Henceforth, we present the result with 63482 particles, which we trust to be robust. By convention, the particle trajectories and their transport are described as forward-in-time in the following sections.

## 3 Routes of the upper limb of the MOC

The MOC upper limb pathways are quantified by considering the subsets of trajectories connecting the exit section (6°S) with each of the entry sections. Figure 2 shows the transport streamfunction (contours) obtained by summing vertically the particles in bins of 1° × 1°, weighted by their transport (magnitude and sign). The sign convention for the transport streamfunction is for forward-in-time trajectories. The color shading shows the depth of the $\sigma_2 = 36.6\text{kg/m}^3$ surface, averaged over the 24-years period covered by ECCOv4. The transport streamfunction flows around the edge of the Southern Ocean supergyre, whose shape is highlighted by the depth contours of the $\sigma_2 = 36.6\text{kg/m}^3$ (Speich et al., 2001, 2002, 2007). All trajectories converge to the region separating the subtropical and tropical gyres in the South Atlantic before reaching 6°S. The net transport at the exit section is composed of:

**DP** 2.0 Sv across Drake Passage at 66°W;
**IT** 4.8 Sv across the Indonesian Throughflow at 116°E;
**TL** 6.6 Sv at 130°E, south of Australia (Tasman Leakage);
**6°S** 0.2 Sv at 6°S flowing southward at depths below the $\sigma_2 = 36.6\text{kg/m}^3$ surface.

Trajectories that enter through DP flow around the edge of the subtropical gyres of the South Atlantic and of the South Indian Ocean before moving northward across the exit section at 6°S, so that a large fraction of the particles entering DP (80% or 1.6 Sv) subsequently go through the Agulhas current region at the tip of South Africa. This pathway has been termed the "indirect cold route" (Gordon et al., 1992) and has a typical transit time longer than 25 years, shown by the secondary peaks in the distribution on the bottom panel of figure 3. The direct cold route, which avoids the Agulhas Current, is a small fraction (20% or 0.4Sv), with typical transit times of 12 years.

Most trajectories come through the Tasman Leakage and the Indonesian throughflow, all steered by the flow around the outer edge of the supergyre. Interestingly, the TL entry section carries more transport (6.6Sv) than the IT (4.8Sv), while the opposite is true in previous analyses (Speich et al., 2001). Our estimate of the median transit time (see figure 3) is 30 years for DP and IT, and 33 years for TL. Both median transit times are substantially shorter than those of Speich et al. (2001), who found 52 years for DP and IT, and 81 years for TL. Furthermore, the e-folding time of the transit-time distribution across TL is shorter (30 years) than the e-folding time across IT (47 years). In all cases, there are long tails in the transit-time distributions, indicating extensive recirculations.

The total transport entering the South Atlantic from the east at 22°E (the tip of South Africa) carries 97% of the transport, while DP through the direct cold route only carries 3% of the MOC. These results should be compared with the partition found in the analysis of an eddy-resolving simulation (Rühs et al., 2019), which finds a 60-40% split between these two routes, i.e. ten times what we find for the direct cold route. One reason for this difference is that ECCOv4 has a stronger climatological eastward transport of the Antarctic Circumpolar Current at Drake passage (155 Sv) than the eddy-resolving, non-assimilative model simulation of Rühs et al. (2019) (116 Sv) – allowing ECCOv4 to carry trajectories that cross DP away from the South Atlantic more efficiently, and perhaps more realistically.

## 4 Thermodynamic properties of the upper limb of the MOC

The thermodynamic characteristics at the entry regions differ markedly between DP, IT and TL. The right panels in figure 4 show the potential temperature-salinity ($\theta - S$) volumetric diagram (colored points, weighted by transport), for the particles at three entry regions, plus at the Agulhas section at 22°E (boxed inset in bottom right panel). The water at DP is cold (mean temperature = 2.3°C) and fresh (mean salinity = 34.3 PSU); the water at the IT is warm (mean temperature = 17.2°) and slightly saltier (mean salinity = 34.4 PSU); the water at TL is intermediate in temperature between DP and IT (mean temperature = 8.7°C) and saltier (mean salinity = 34.6 PSU). The TL water includes a fraction which shares the properties originating at the Drake Passage, i.e. cold and relatively fresh: this water is associated with the outer streamlines (positive near zero values), which flow eastward in the southern region of the ACC and then turn around to enter the TL section.

As in the original "warm-cold route" nomenclature (Gordon, 1986), there is a substantial difference in temperature between the waters originating in DP and those originating in IT and TL, while the distinction in salinity is not as pronounced. However, by the time the particles reach 6°S the differences between these characteristics are erased and the three groups are undistinguishable in $\theta - S$ space, as found in Rühs et al. (2019). This is because all trajectories eventually merge into the narrow South Equatorial Current and North Brazil Current before reaching 6°S. This merger facilitates property transformations along isopycnals. Properties are also transformed through diapycnal mixing and air-sea interaction across isopycnals. Furthermore, the IT, TL and "indirect-route" DP waters are all eventually squeezed into the narrow Agulhas Current system, from which they emerge as a single water mass in the South Atlantic, with a tight $\theta - S$ relation at 22°E (the boxed inset in the bottom right panel of figure 4), with an average salinity of 35 PSU.

The bulk of particles arriving at 6°S have a salinity near 35.6 PSU which is larger than any of the water masses at their sections of origin, or at 22°E. This requires loss of freshwater in the journey to and across the South Atlantic in this region that loses a total of 0.44 Sv of freshwater at the surface. The net surface evaporation is consistent with an increase in La-

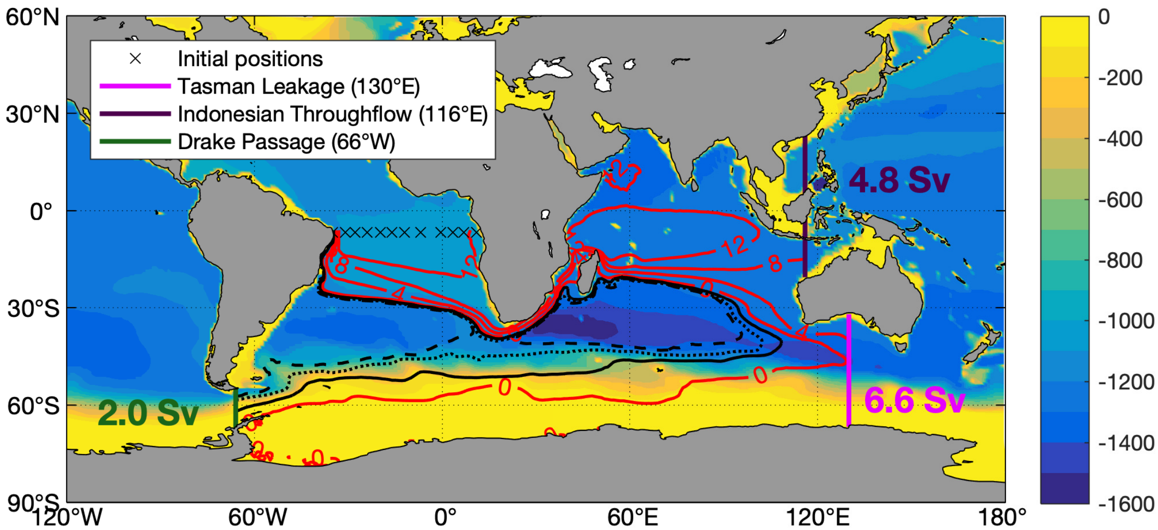


**Figure 2.** Transport streamfunction calculated from particle trajectories (contours): red contours are 4Sv apart; the black solid contour is -1Sv, the black dotted contour is -1.5Sv and the black dashed contour is -1.75Sv. The color shading shows the depth (in m) of the time-averaged $\sigma_2$=36.6 kg/m$^3$. The exit section at 6°S is marked by black x, and the entry sections are at Drake passage (66°W green), at Tasman Leakage (130°E magenta), and Indonesian Throughflow (116°E dark purple). The transport at each entry section is marked in the corresponding color. The transport at the exit section is 13.6Sv. After 2011 years there are 0.04Sv still recirculating in the region bounded by the four sections, and 0.2Sv have entered 6°S from the North below $\sigma_2$=36.6 kg/m$^3$.

grangian transport of salinity between the entry and exit regions of 16.6 PSU Sv, which is equivalent to a mass evaporation of 0.46 Sv at an average surface salinity of 36 PSU.

While the particles become saltier from their region of origin at DP, IT and TL, the particles from DP and TL become sufficiently warmer to overcome the density increase due to salinification. The net result is that, with the exception of the particles originating in the IT, the particles at 6°S become less dense than at their origin. The particles originating at the IT experience a general cooling as they pass through the Agulhas Current system, only to be warmed up again in the South Atlantic. Typical trajectories from the entry regions of TL, IT, DP (including both direct and indirect route) to the exit region are shown in the supplemental material. The animations provide a visualization of both time scales and pathways, while also revealing salinity and potential temperature transformations along the trajectories.

The particles entering the South Atlantic through the "warm route" have an average salinity of 35 PSU at 22°E (the Agulhas region), i.e. slightly saltier than the average salinity of NADW, which is 34.9 PSU (as quantified by the average salinity water at 6°S with densities larger than $\sigma_2 = 36.6$kg/m$^3$). The upper branch of the MOC gets saltier as it flows northward,

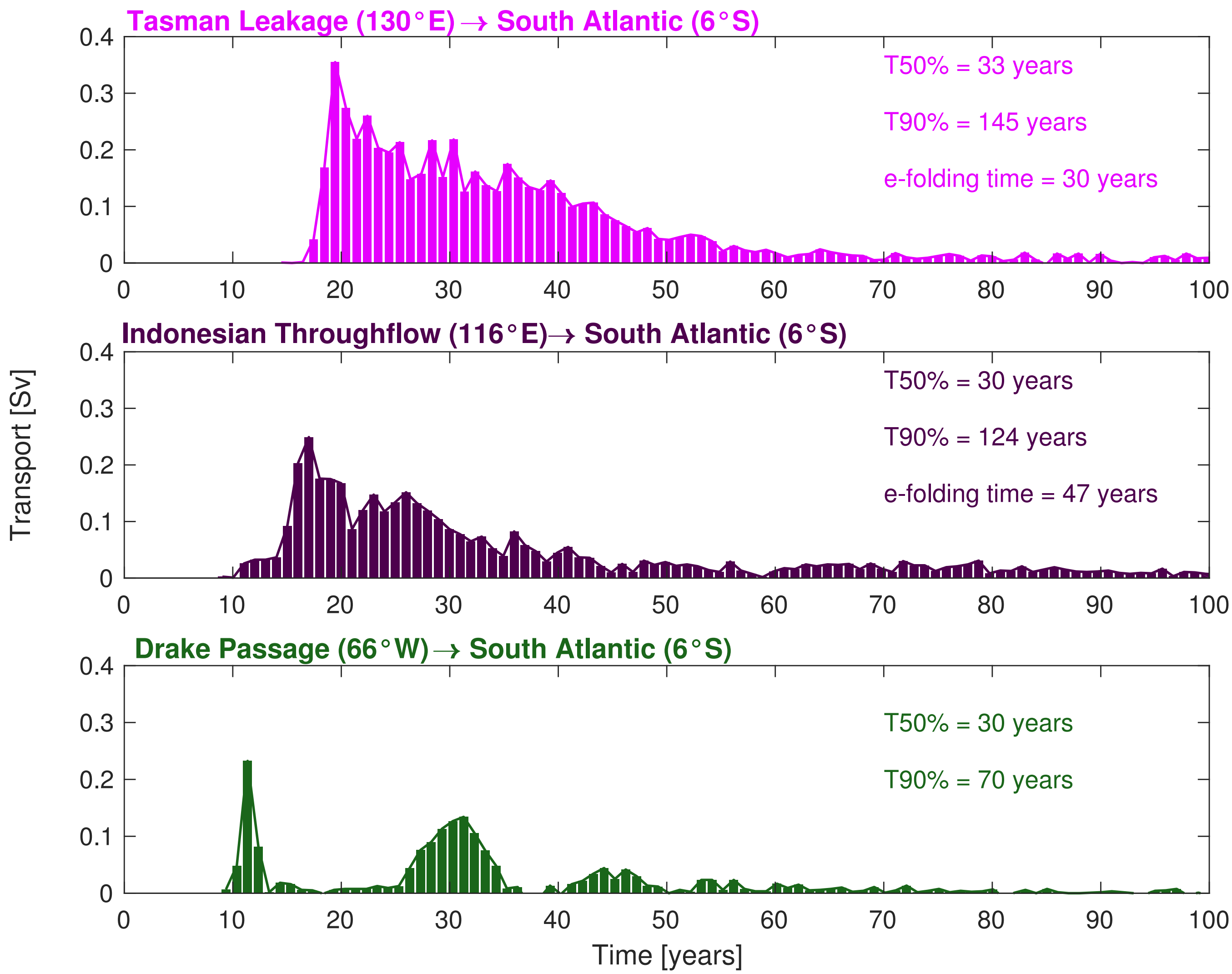


**Figure 3.** Distribution of transit times from the exit to each entry section weighted by transport. The inset also shows the median, the 90th percentile and the e-folding time-scales fitted to the distributions between 9 and 150 years.

reaching 35.6 PSU at 6°S, so that it is saltier than NADW at both 30°S and 6°S, thus exporting freshwater out of the North Atlantic sector.

## 5 Conclusions

Based on a state estimate which is a close fit to most available global data constraints, we evaluate the routes and thermohaline properties of the upper branch of the MOC using a Lagrangian analysis using the three-dimensional velocities of ECCOv4. We find that the upper branch of the MOC receives its transport primarily from the region south of Australia (Tasman Leakage), followed by a close second contribution at the Indonesian Throughflow, and a distant third contribution from Drake Passage.

Eighty percent of the particle transport through 6°S originating from Drake Passage goes through the indirect cold route. This tortuous path results in a loss of identity in $\theta-S$ space. Indeed all three contributions have essentially the same properties when entering the South At-

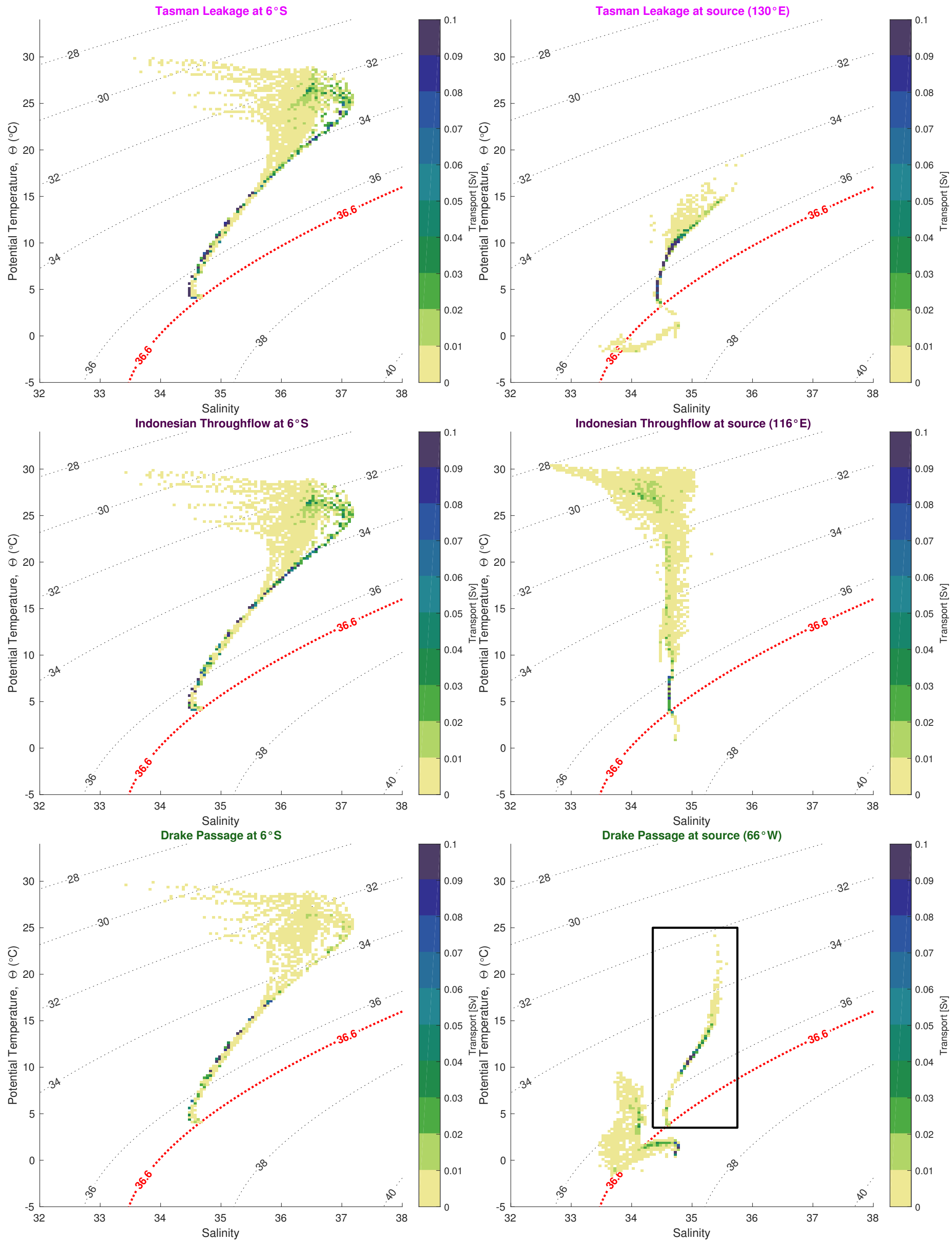


**Figure 4.** Particle transports binned in potential temperature/salinity space following particles at the entry (right) and exit (left) sections. Particles entering from Tasman Leakage are in the top row, from Indonesian Throughflow in the middle row, and from Drake passage in the bottom row. The boxed inset in the bottom right panel shows the $\theta - S$ relation of the particles crossing the Agulhas section at 22°E, south of Africa. This entry section carries 13.2 Sv (97% of the exit transport) compressed in a tight $\theta - S$ relation, regardless of the upstream entry point (DP, IT, or TL). The dashed lines show contours of constant $\sigma_2$.

lantic, casting doubts on the ability to recognize the origin of this transport through comparative analysis of water masses, as remarked in Rühs et al. (2019).

We demonstrate that the MOC exports freshwater out of the North Atlantic sector. This is important because simple models of the MOC indicate that when the MOC exports freshwater out of the Atlantic, the salt-advection feedback is operating, leading to potential bistability of the overturning circulation (Stommel, 1961; de Vries & Weber, 2005; Beal et al., 2011; Drijfhout et al., 2011).

**Acknowledgments**

Support by the National Science Foundation under Grant OCE-1634128 and by the National Aeronautic and Space Administration under grant 80NSSC20K0796 is gratefully acknowledged. Computational resources were provided by the Extreme Science and Engineering Discovery Environment (XSEDE) on Stampede2 at the Texas Advanced Computing Center through allocation TG-OCE130026. XSEDE is supported by the National Science Foundation grant number ACI-1548562. The ECCOv4 data can be downloaded from `ftp://ecco.jpl.nasa.gov/Version4/Release3/`, while the MITgcm FLT package can be downloaded from `https://github.com/MITgcm/MITgcm/tree/master/pkg/flt`.

## References

Beal, L. M., Ruijter, W. D., Biastoch, A., Zahn, R., Cronin, M., Hermes, J., ... others (2011). On the role of the Agulhas system in ocean circulation and climate. *Nature*, *472*, 429.

Blanke, B., & Raynaud, S. (1997). Kinematics of the Pacific Equatorial Undercurrent: An Eulerian and Lagrangian approach from GCM results. *J. Phys. Oceanogr.*, *27*(6), 1038-1053.

Cessi, P. (2019). The Global Overturning Circulation. *Annual review of marine science*, *11*, 249–270.

Cessi, P., & Jones, C. (2017). Warm-route versus cold-route interbasin exchange in the meridional overturning circulation. *J. Phys. Oceanogr.*, *47*, 1981–1997.

Cunningham, S., Alderson, S., King, B., & Brandon, M. (2003). Transport and variability of the Antarctic Circumpolar Current in Drake Passage. *J. Geophys. Res.: Oceans*, *108*(C5).

de Vries, P., & Weber, S. L. (2005). The Atlantic freshwater budget as a diagnostic for the existence of a stable shut down of the meridional overturning circulation. *Geophys. Res. Lett.*, *32*, L09606.

Donners, J., & Drijfhout, S. (2004). The Lagrangian view of South Atlantic interocean exchange in a global ocean model compared with inverse model results. *J. Phys. Oceanogr.*, *34*, 1019–1035.

Donohue, K., Tracey, K., Watts, D., Chidichimo, M. P., & Chereskin, T. (2016). Mean Antarctic Circumpolar Current transport measured in Drake Passage. *Geophys. Res. Let.*, *43*, 11–760.

Döös, K. (1995). Interocean exchange of water masses. *J. Geophys. Res.*, *100*, 13499–13514.

Drijfhout, S., Weber, S. L., & van der Swaluw, E. (2011). The stability of the MOC as diagnosed from model projections for pre-industrial, present and future climates. *Clim. Dyn.*, *37*, 1575-1586.

Forget, G., Campin, J.-M., Heimbach, P., Hill, C. N., Ponte, R. M., & Wunsch, C. (2015). ECCO version 4: an integrated framework for non-linear inverse modeling and global ocean state estimation. *Geoscientific Model Development*, *8*(10), 3071–3104. Retrieved from `http://www.geosci-model-dev.net/8/3071/2015/` doi: 10.5194/gmd-8-3071-2015

Forget, G., & Ferreira, D. (2019). Global ocean heat transport dominated by heat export from the tropical Pacific. *Nature Geoscience*. Retrieved from `https://doi.org/10`

.1038/s41561-019-0333-7 doi: 10.1038/s41561-019-0333-7

Forget, G., Ferreira, D., & Liang, X. (2015). On the observability of turbulent transport rates by argo: supporting evidence from an inversion experiment. *Ocean Sci.*, *11*, 839-853.

Forget, G., & Ponte, R. M. (2015). The partition of regional sea level variability. *Progress in Oceanography*, 173–195.

Fukumori, I., Wang, O., Fenty, I., Forget, G., Heimbach, P., & Ponte, R. M. (2017). *Ecco version 4 release 3* (Tech. Rep.).

Gent, P., & McWilliams, J. C. (1990). Isopycnal mixing in ocean circulation models. *J. Phys. Oceanogr.*, *20*, 150-155. doi: 10.1175/1520-0485(1990)020<0150:IMIOCM>2.0.CO;2

Gordon, A. L. (1986). Interocean exchange of thermocline water. *J. Geophys. Res.*, *91*, 5037-5046.

Gordon, A. L., Weiss, R. F., Smethie, W. M., & Warner, M. J. (1992). Thermocline and intermediate water communication between the south atlantic and indian oceans. *J. Geophys. Res.*, *97*, 7223–7240.

Griffies, S. M. (1998). The Gent-McWilliams skew flux. *J. Phys. Oceanogr.*, *28*(5), 831-841.

Holfort, J., & Siedler, G. (2001). The meridional oceanic transports of heat and nutrients in the South Atlantic. *J. of Phys. Oceanogr.*, *31*, 5–29.

Hsiung, J. (1985). Estimates of global oceanic meridional heat transport. *J. Phys. Oceanogr.*, *15*, 1405-1413.

Jackson, L. C., Dubois, C., Forget, G., Haines, K., Harrison, M., Iovino, D., … Zuo, H. (2019). The mean state and variability of the north atlantic circulation: A perspective from ocean reanalyses. *J. Geophys. Res.: Oceans*, *124*(12), 9141-9170. doi: 10.1029/2019JC015210

Kang, S. M., Held, I. M., Frierson, D. M. W., & Zhao, M. (2008). The response of the ITCZ to extratropical thermal forcing: Idealized slab-ocean experiments with a GCM. *J. Climate*, *21*, 3521-3532.

Macdonald, A. M. (1998). The global ocean circulation: A hydrographic estimate and regional analysis. *Progress in Oceanography*, *41*(3), 281–382.

Redi, M. H. (1982). Oceanic isopycnal mixing by coordinate rotation. *J. Phys. Oceanogr.*, *12*, 1154-1158. doi: 10.1175/1520-0485(1982)012<1154:OIMBCR>2.0.CO;2

Rintoul, S. R. (1991). South Atlantic interbasin exchange. *J. Geophys. Res.*, *96*, 2675-2692.

Rodrigues, R. R., Wimbush, M., Watts, D. R., Rothstein, L. M., & Ollitrault, M. (2010). South Atlantic mass transports obtained from subsurface float and hydrographic data. *J. of Mar. Res.*, *68*, 819–850.

Rühs, S., Schwarzkopf, F. U., Speich, S., & Biastoch, A. (2019). Cold vs. warm water route – sources for the upper limb of the atlantic meridional overturning circulation revisited in a high-resolution ocean model. *Ocean Science*, *15*(3), 489–512. Retrieved from https://www.ocean-sci.net/15/489/2019/ doi: 10.5194/os-15-489-2019

Schmitz Jr, W. J. (1995). On the interbasin-scale thermohaline circulation. *Reviews of Geophysics*, *33*(2), 151–173.

Sloyan, B. M., & Rintoul, S. R. (2001). Circulation, renewal, and modification of Antarctic Mode and Intermediate Water. *J. Phys. Oceanogr.*, *31*(4), 1005-1030.

Speich, S., Blanke, B., & Cai, W. (2007). Atlantic meridional overturning circulation and the southern hemisphere supergyre. *Geophys. Res. Lett.*, *34*, L23614. doi: doi:10.1029/2007GL031583

Speich, S., Blanke, B., de Vries, P., Drijfhout, S., Döös, K., Ganachaud, A., & Marsh, R. (2002). Tasman leakage: A new route in the global ocean conveyor belt. *Geophys. Res. Lett.*, *29*(10), 55-1–55-4.

Speich, S., Blanke, B., & Madec, G. (2001). Warm and cold water routes of an ogcm thermohaline conveyor belt. *Geophys. Res. Lett.*, *28*, 311–314.

Stommel, H. (1961). Thermohaline convection with two stable regimes of flow. *Tellus*, *13*, 224-230.

Talley, L. D. (2013). Closure of the global overturning circulation through the Indian, Pacific, and Southern Oceans: Schematics and transports. *Oceanography*, *26*(1), 80-97. doi: 10.5670/oceanog.2013.07

Uotila, P., Goosse, H., Haines, K., Chevallier, M., Barthélemy, A., Bricaud, C., … others (2019). An assessment of ten ocean reanalyses in the polar regions. *Clim. Dyn.*, *52*, 1613–1650.

Young, W. R. (2012). An exact thickness-weighted average formulation of the Boussinesq equations. *J. Phys. Oceanogr.*, *42*(5), 692-707.